

# Defect Control in a Selective Reduction Reaction to Synthesize a Metal/Ceramic Nanocomposite

Tomohiro Suetsuna,<sup>†</sup> Takayuki Fukasawa, Seiichi Suenaga, and Koichi Harada

Functional Materials Laboratory, Corporate Research & Development Center, Toshiba Corporation, Kanagawa 212-8582, Japan

**A metal/ceramic nanocomposite was synthesized by defect control in a selective reduction reaction of a complex solid solution. The defect type of a (Co, Mg)O solid solution was controlled by doping oxides with different valencies. The controlled defects strongly affected the reduction reaction behaviors as well as material morphologies after the reaction. In the case of scandium doping, the diffusion was rate controlling in the reduction reaction, and metals of a nanocolumn-like structure were highly dispersed into the matrix. On the other hand, in the case of lithium doping, the interface reaction was rate controlling in the reaction, and metal nanoparticles were highly dispersed into the matrix.**

## I. Introduction

COMPOSITE materials, such as metal/ceramic and metal/polymers, offering multifunctionality and superior physical properties, are expected to be used for various applications. For example, metal nanoparticles embedded in a ceramic can improve or modify the mechanical, optical, electrical, and magnetic properties of the ceramic.<sup>1–7</sup> The metal nanoparticles also become stable in a matrix such as a ceramic and a polymer, although their oxidation resistance and thermal stability are quite low when their sizes are of a nanoscale order. Therefore, peculiar physical properties of metal nanoparticle such as size effect and excellent catalytic property can be obtained by embedding it into the matrix. These advantages of composite materials can be obtained by controlling the material morphology and interface structure at the nanoscale, and process development of the composite material is very important.

One of the effective methods to produce metal nanoparticles embedded in a matrix is the selective reduction reaction method from a complex solid solution, which is composed of a stable and unstable oxide in a reducing atmosphere.<sup>1–12</sup> In this method, metal nanoparticles are deposited selectively from an unstable oxide in a complex solid solution in a reducing atmosphere. Previous studies revealed that nickel or cobalt nanoparticles could be deposited on the surface of an oxide matrix by reducing (Ni, Mg)O or (Co, Mg)O solid solutions.<sup>1–12</sup> However, almost all the metal particles in these studies were deposited on the surface of grain boundaries of the matrix, and not into the grain. Therefore, the packing densities of metal particles into the oxide were low, and insufficient for applications such as particulate recording media, where the large packing density of metal particles is important.<sup>2,3</sup> Also, the deposited metal particles in the previous studies have either cubic or spherical structures.<sup>1–12</sup> Because the shape of metal particles generally affects physical properties such as the electrical and magnetic properties, it is

important to increase variation of the morphologies in metal/ceramic composite materials.

The objective of the present research is to investigate the reduction reaction behavior of the (Co, Mg)O solid solution system in a hydrogen atmosphere, and to increase the variation of the morphologies in the metal/ceramic nanocomposite material by controlling defects in the solid solution. The defect type of (Co, Mg)O solid solution was controlled by doping an oxide with different valencies. It was found that the reduction behaviors of (Co, Mg)O as well as the morphologies after the reduction were drastically modified by controlling the defect in (Co, Mg)O.

## II. Experimental Procedure

The raw materials used for the present research were MgO (500A, Ube Material Industries, Ltd., Ube, Japan; >99.9% purity, <0.1- $\mu\text{m}$  particle size), CoO (NanoTek CoO-2, C.I. Kasei Co. Ltd., Tokyo, Japan; >99% purity (CoO:Co<sub>3</sub>O<sub>4</sub> = 55:44), <0.1- $\mu\text{m}$  particle size), Sc<sub>2</sub>O<sub>3</sub> (45940F, Kojundo Chemical Lab. Co. Ltd., Saitama, Japan; 99.99% purity, 1–3- $\mu\text{m}$  particle size), and Li<sub>2</sub>CO<sub>3</sub> (126-01135, Wako Pure Chemical Industries Ltd., Osaka, Japan; 99% purity) powders. Sc<sub>2</sub>O<sub>3</sub> and Li<sub>2</sub>CO<sub>3</sub> were selected as doping oxides with different valencies (trivalent and monovalent) from those of CoO and MgO (divalent). Among the various trivalent oxides, Sc<sub>2</sub>O<sub>3</sub> is distinguished by its small ionic radius and the ease with which relatively large amounts of Sc<sub>2</sub>O<sub>3</sub> can be solved into another oxide.<sup>13</sup> These powders (CoO, MgO, Sc<sub>2</sub>O<sub>3</sub>, and Li<sub>2</sub>CO<sub>3</sub>) were mixed at a given composition in ethanol for 24 h using a ball mill, and the mixed powders were sieved to 200  $\mu\text{m}$  after removing ethanol. These powders were sintered in air at 1400°C for 20 h in a furnace (MSTF-1530, Yamada Denki Co. Ltd., Tokyo, Japan) to produce (Co, Mg)O solid solution powders with and without Sc<sub>2</sub>O<sub>3</sub> or Li<sub>2</sub>O as a doping oxide (Li<sub>2</sub>CO<sub>3</sub> was changed to Li<sub>2</sub>O during sintering in air at 1400°C for 20 h. Co<sub>3</sub>O<sub>4</sub> was also changed to CoO during the sintering). Each powder was ground and 50 mg of it was reduced in flowing hydrogen (at a flowing rate of 100 sccm) using a thermogravimetric analyzer system (TG; TGD-9600 and MTS-9000, ULVAC-RIKO Inc., Yokohama, Japan). The heating rate was 15°C/min for the investigation of the reduction reaction behavior over a wide range of temperatures up to 1000°C and 200°C/min for the investigation of the reaction rate constant at a specific temperature. It was investigated for the reaction behavior from 7 to 13 wt% reduction in order to obtain a uniform sample temperature.

The real densities of the sintered powders were examined by a pycnometer (Micromeritics Gas Pycnometer Accupyc 1330-01, Shimadzu Analytical & Measuring Center Inc., Tokyo, Japan) using helium gas. About 7 g of each of the sintered powders was used for the density measurements after they were ground and heated in vacuum at 200°C for 1 h. Their compositions were examined by an inductive-coupled plasma spectrometer (ICP; ICPS-8000, Shimadzu Analytical & Measuring Center Inc.). Crystalline phases were identified by X-ray diffractometry (XRD; M18XHF<sup>22</sup>-SRA, MacScience Co. Ltd., Yokohama, Japan), using CuK $\alpha$  radiation at 40 kV and 100 mA. Lattice

L. Klein—contributing editor

Manuscript No. 23016. Received April 2, 2007; approved June 11, 2007.

<sup>†</sup>Author to whom correspondence should be addressed. e-mail: tomohiro.suetsuna@toshiba.co.jp

**Table I. Information on the (Co, Mg)O Samples Sintered at 1400°C for 20 h**

Sample No.	Lattice constant (Å)	Density (g/cm <sup>-3</sup> )	Co:Mg:Sc (or Li) ratio	Crystalline phase
1	4.25298 ± 0.00043	5.8574 ± 0.0038	4.02:1:0 (without additive)	Only solid solution
2	4.25427 ± 0.00072	5.8434 ± 0.0023	3.98:1:0.00973 (Sc)	Only solid solution
3	4.25581 ± 0.00053	5.7495 ± 0.0032	3.99:1:0.104 (Sc)	Solid solution+Sc <sub>2</sub> O <sub>3</sub> (little)
4	4.25271 ± 0.00024	5.8475 ± 0.0030	4.02:1:0.00497 (Li)	Only solid solution
5	4.24929 ± 0.00058	5.8191 ± 0.0040	4.04:1:0.0557 (Li)	Only solid solution
6	4.24699 ± 0.00047	5.7160 ± 0.0036	4.03:1:0.142 (Li)	Only solid solution

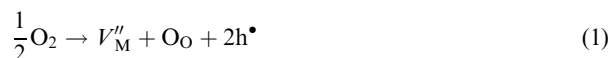
constants were examined by mixing the sample powders with silicon standard powder (640c, National Institute of Standards & Technology, Gaithersburg, MD; lattice constant at 22.5°C is 5.4311946 ± 0.0000092 Å). The nanostructures and compositions of both sintered and reduced powders were examined by scanning electron microscopy (SEM; JSM-840F, JEOL Ltd., Tokyo, Japan) and transmission electron microscopy (TEM; JEM-2000EX and JEM-2000FX, JEOL Ltd.) with an accelerating voltage of 200 kV, and energy-dispersive spectroscopy (EDS; JEM-2000FX, JEOL Ltd., and Link-ISIS, Oxford Instruments plc, Abingdon, U.K.).

### III. Results and Discussion

#### (1) Synthesized Solid Solution

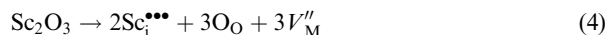
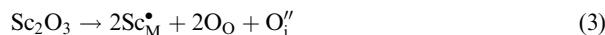
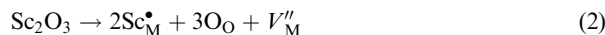
The information on the (Co, Mg)O samples (named Sample No. 1–6) sintered in air at 1400°C for 20 h is shown in Table I. The ratio of cobalt to magnesium in all the samples was about 4. The crystalline phase of all the samples except Sample No. 3 was only the (Co, Mg)O solid solution phase. In Sample No. 3, a small amount of a Sc<sub>2</sub>O<sub>3</sub> phase as well as a (Co, Mg)O solid solution phase was detected, because the doping concentration of scandium ion in (Co, Mg)O was sufficient to exceed the solid solubility limit.<sup>13</sup> As the doping concentration of scandium ion in (Co, Mg)O increased, the lattice constant of the (Co, Mg)O solid solution increased and the real density decreased. On the other hand, as the doping concentration of lithium ion increased, both the lattice constant and real density decreased. Figures 1 and 2 show the dependence of the doping ratio on the experimental and calculated density of the sintered (Co, Mg)O samples (Fig. 1 is for the case in which Sc<sub>2</sub>O<sub>3</sub> was the doping oxide and Fig. 2 is for the case in which Li<sub>2</sub>O was the doping oxide). The calculated density was obtained from the experimental composition (Co:Mg:Sc(or Li) ratio) and lattice constant, considering the following model.

(A) *Without Dopant:* Both CoO and MgO are *p*-type oxides, which easily form metal cation vacancy. Assuming that the synthesized (Co, Mg)O are also a *p*-type oxide, the defect would be formed in accordance with the following equation:



where M is the metal cation of the (Co, Mg)O solid solution. Assuming that cobalt and magnesium equally have a metal cation vacancy, the composition of the synthesized (Co, Mg)O was (Co<sub>0.79748</sub>, Mg<sub>0.19817</sub>)O from the experimental composition, lattice constant, and Eq. (1).

(B) *With Scandium as a Dopant:* In the (Co, Mg)O solid solution, the metal cations are divalent, whereas the scandium ion of the doping oxide is trivalent. Therefore, when the scandium ion is solved into the (Co, Mg)O, the defect would be formed in accordance with the following Eqs. (2)–(4) or (5) because the total charge remains neutral:



Equations (2) and (3) apply when a metal cation of (Co, Mg)O is displaced by a scandium ion of the doping oxide. Metal cation vacancy is formed in accordance with Eq. (2), and interstitial oxygen is formed in accordance with Eq. (3). Eqs (4) and (5) apply when the scandium ion of the doping oxide becomes an interstitial ion. Metal cation vacancy is formed in accordance

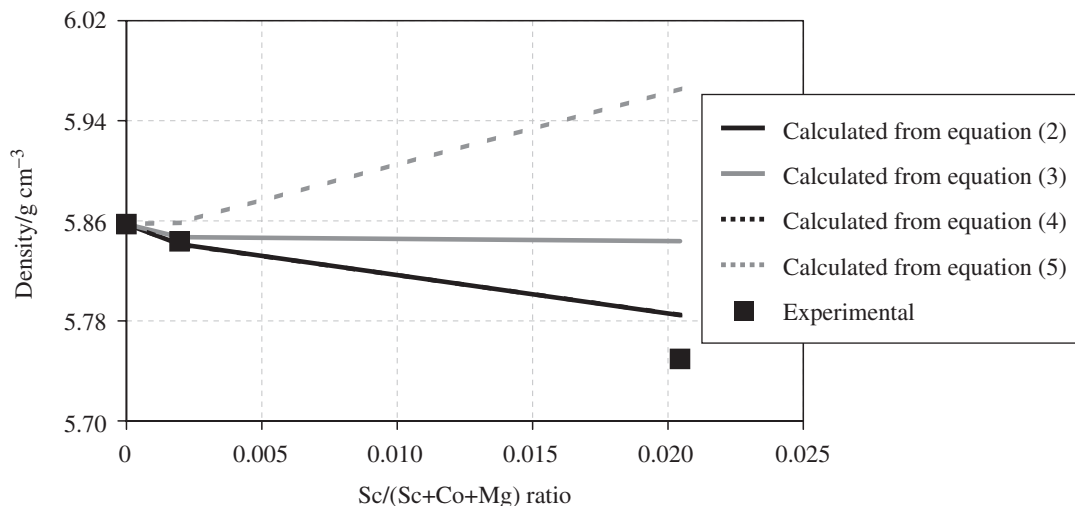


**Fig. 1.** Sc/(Sc+Co+Mg) ratio dependence on the experimental and calculated density of the (Co, Mg)O samples sintered at 1400°C for 20 h. The line of Eq. (2) is the same as that of Eq. (4).

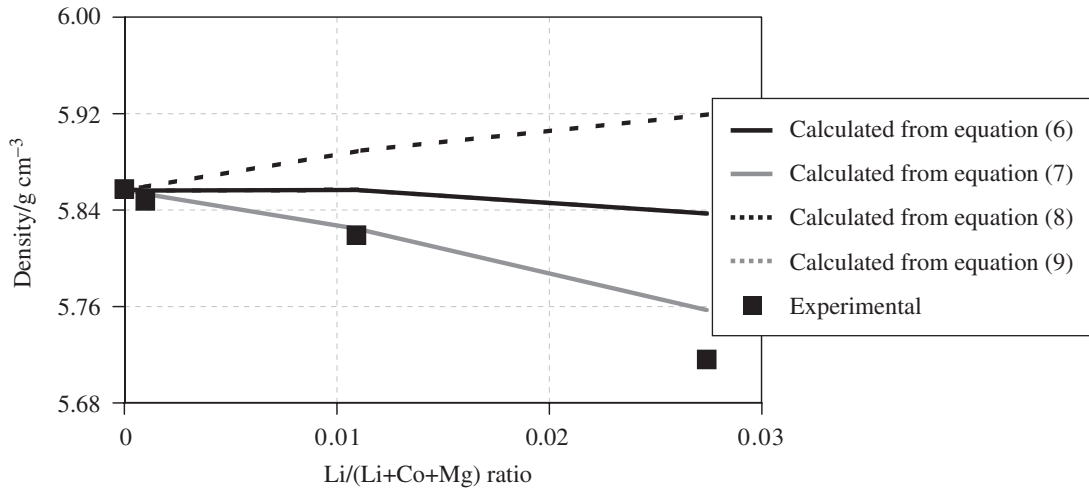


Fig. 2. Li/(Li+Co+Mg) ratio dependence on the experimental and calculated densities of the (Co, Mg)O samples sintered at 1400°C for 20 h. The line of Eq. (6) is the same as that of Eq. (9).

with Eq. (4), and interstitial oxygen is formed in accordance with Eq. (5). The calculated densities were obtained from the experimental composition, lattice constant, and Eqs. (2)–(4) or (5) shown as dotted or solid lines in Fig. 1. From Fig. 1, the experimental density is in relatively good agreement with the calculated ones in the case of Eqs. (2) or (4); the metal cation of (Co, Mg)O is displaced by the scandium ion of the doping oxide or the scandium ion becomes an interstitial ion to form a metal cation vacancy. It was found that the concentration of the metal cation vacancy increased as the doping concentration of the scandium ion increased.

(C) *With Lithium as a Dopant:* When lithium ion is solved into the (Co, Mg)O, the defect would be formed in accordance with the following equations:



Equations (6) and (7) apply when a metal cation of (Co, Mg)O is displaced by the lithium ion of the doping oxide. Interstitial metal cation is formed in accordance with Eq. (6), and an oxygen vacancy is formed in accordance with Eq. (7). Equations (8) and (9) apply when the lithium ion of the doping oxide becomes an interstitial ion. An interstitial oxygen ion is formed in accordance with Eq. (8), and a metal cation vacancy is formed

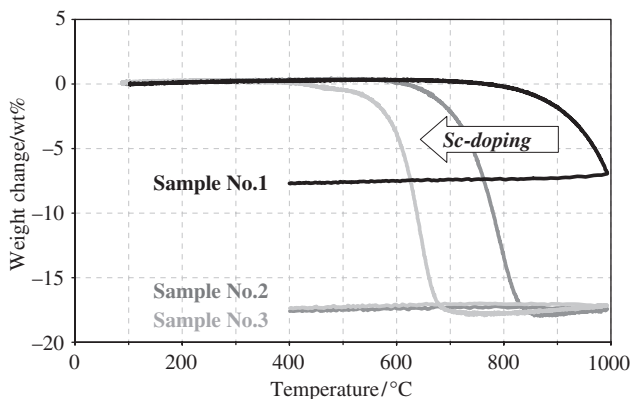


Fig. 3. Weight change behaviors of the scandium-doped and undoped (Co, Mg)O samples at up to 1000°C in flowing hydrogen.

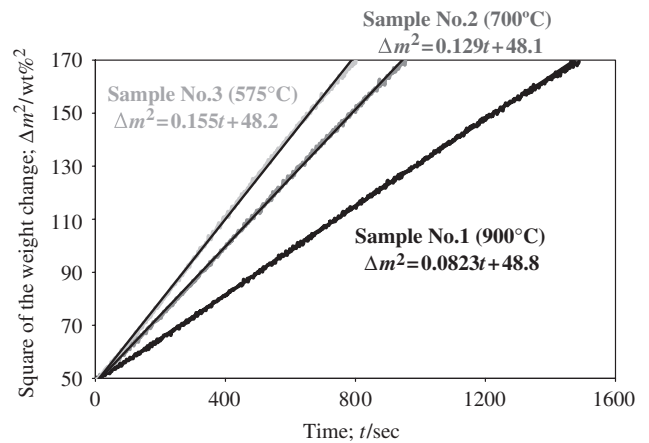


Fig. 4. Weight change behaviors of the scandium-doped and undoped (Co, Mg)O samples in the flowing hydrogen as a function of time at a specific temperature. Regression lines are also shown as black lines.

in accordance with Eq. (9). The calculated densities were obtained from the experimental composition, lattice constant, and Eqs. (6)–(8), or (9) shown as dotted or solid lines in Fig. 2. From Fig. 2, the experimental density was in relatively good agreement with the calculated one in the case of Eq. (7); the metal cation of (Co, Mg)O is displaced by the lithium ion of the doping oxide to form an oxygen ion vacancy. It was found that the concentration of oxygen ion vacancy increased as the doping concentration of lithium ion increased.

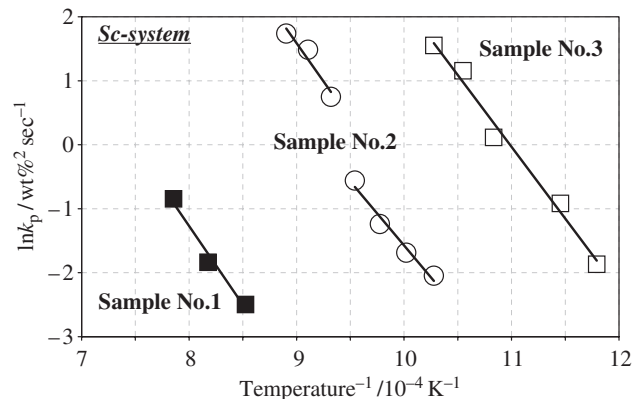
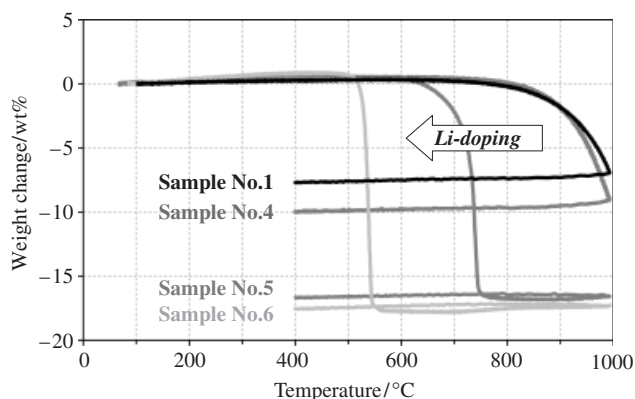


Fig. 5. Arrhenius plots of the hydrogen-reduction reaction of the scandium-doped and undoped (Co, Mg)O samples: Sample No. 1 (■), Sample No. 2 (○), Sample No. 3 (□).

**Table II. Activation Energy and Frequency Factor (with  $\pm 1$  Standard Error) of Hydrogen-Reduction Reaction of the Doped and Undoped (Co,Mg)O Samples Sintered at 1400°C for 20 h**

Sample No.	Temperature range (°C)	Reduction behavior	Activation energy (kJ/mol)	Frequency factor
1	900–1000	Parabolic	$204 \pm 29$	$9.75 \times 10^7 \pm 1.66 \times 10^1$ (wt% <sup>2</sup> /s)
2	700–775	Parabolic	$166 \pm 20$	$9.65 \times 10^7 \pm 1.07 \times 10^1$ (wt% <sup>2</sup> /s)
	800–850	Parabolic	$199 \pm 54$	$1.06 \times 10^{10} \pm 3.53 \times 10^2$ (wt% <sup>2</sup> /s)
3	575–700	Parabolic	$186 \pm 12$	$5.02 \times 10^{10} \pm 5.12$ (wt% <sup>2</sup> /s)
4	850–950	Parabolic	$127 \pm 6$	$9.30 \times 10^4 \pm 1.89$ (wt% <sup>2</sup> /s)
5	700–800	Linear	9.69	1.19 (wt%/s)
6	600–700	Linear	12.7	2.39 (wt%/s)



**Fig. 6.** Weight change behavior of the lithium-doped and undoped (Co, Mg)O samples at up to 1000°C in flowing hydrogen.

## (2) Reduction Reaction Behavior

The (Co, Mg)O solid solution samples were reduced in flowing hydrogen. The hydrogen-reduction reaction behaviors of the scandium-doped (Co, Mg)O solid solution are shown in Fig. 3. The behavior of the undoped (Co, Mg)O solid solution is also shown in Fig. 3. From Fig. 3, it can be seen that as the doping concentration of scandium ion increased, the temperature from which reduction started drastically decreased. Figure 4 shows the weight change behavior as a function of reduction time at a specific temperature. The reduction reaction behaviors through-

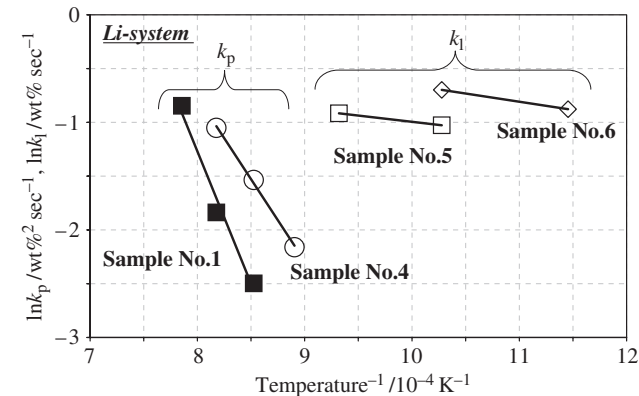
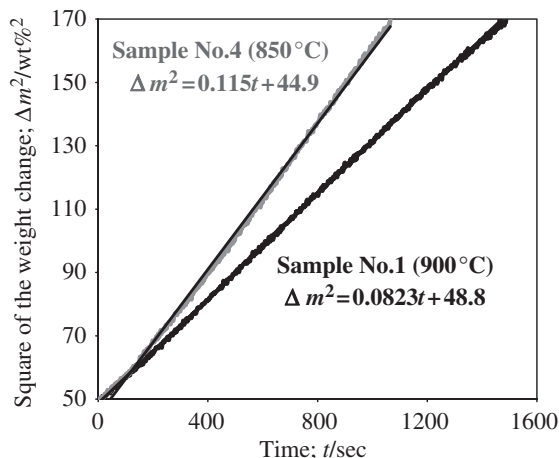


**Fig. 8.** Arrhenius plots of the hydrogen-reduction reaction of the lithium-doped and undoped (Co, Mg)O samples: Sample No. 1 (■), Sample No. 4 (○), Sample No. 5 (□), Sample No. 6 (□).

out the scandium-doping system (including the sample without doping oxide) obeyed a parabolic law as follows:

$$\Delta m^2 = k_p t \quad (10)$$

where  $\Delta m$  is the weight loss per unit surface area,  $k_p$  is the parabolic reduction reaction rate constant, and  $t$  is the reduction time. This parabolic law indicates that diffusion was rate controlling in the reaction. The reduction reaction rate constant at each temperature was also examined to obtain Arrhenius plots, as shown in Fig. 5. Table II summarizes the activation energy and frequency factor from the Arrhenius plots (the data of lithium-doped samples are also shown in Table II). From Fig. 5 and Table II, the activation energy for reduction reaction decreased slightly and the frequency factor increased as the doping concentration of scandium ion increased. The diffusion rate of the metal cation of the (Co, Mg)O solid solution increased on increasing the metal cation vacancy, which was due to the increasing doping concentration of scandium ion. However, the oxygen ion diffusion or hydrogen diffusion would be rate controlling in the reduction reaction of (Co, Mg)O in this study, because the oxygen ion diffusion is much slower than that of metal cation diffusion if the metal cation vacancy is the dominant defect. Therefore, the increased metal cation diffusion rate would have little effect on the activation energy for the reduction reaction, and would affect the frequency factor because the increased metal cation diffusion rate could increase the possibility of starting a reduction reaction. This increase in the frequency factor could be a reason for the decreased temperature from which reduction started.

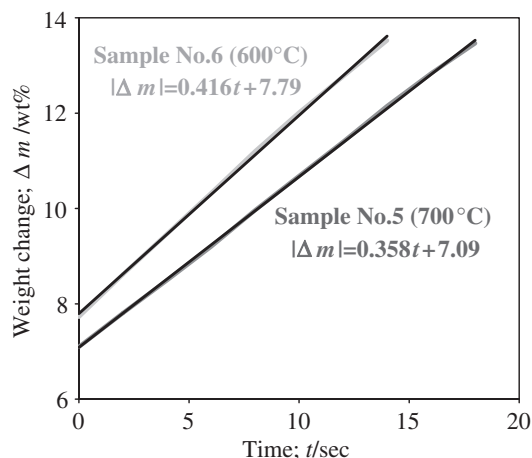


**Fig. 7.** Weight change behaviors of the lithium-doped and undoped (Co, Mg)O samples in the flowing hydrogen as a function of time at a specific temperature. Regression lines are also shown as black lines.

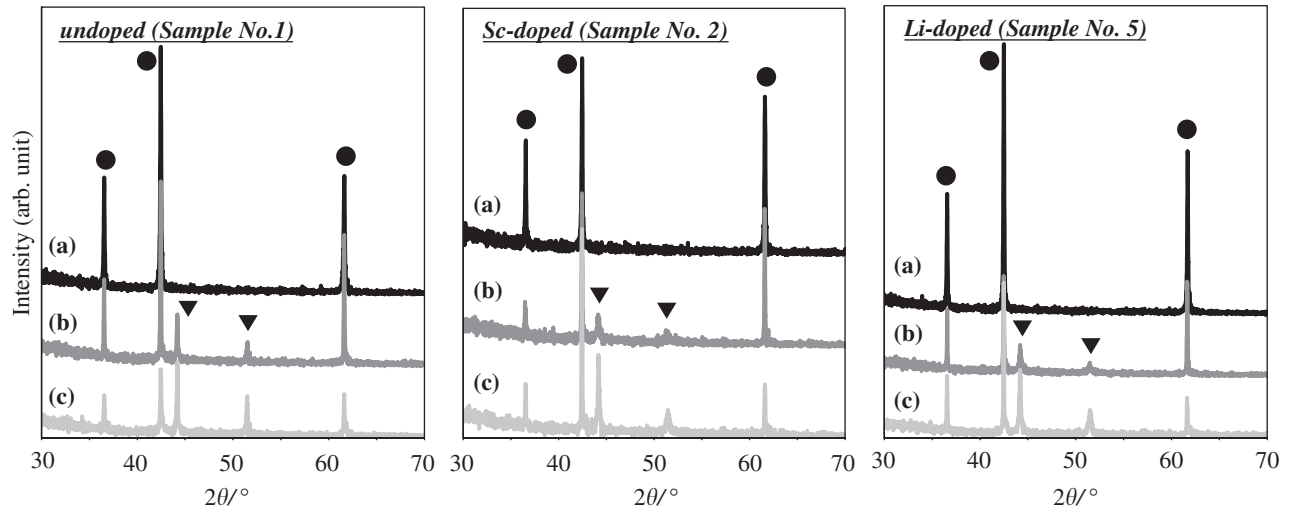


**Fig. 9.** X-ray diffraction patterns of the scandium-doped, lithium-doped, and undoped (Co, Mg)O samples before and after the hydrogen reduction: (a) before reduction, (b) after 2.5–3 wt% reduction, (c) after 5.5–6 wt% reduction (reduction temperature was 1000°C in the case of the undoped sample, and 750°C in the case of the doped ones) ●, (Co, Mg)O solid solution; ▼, Co (15-0806).

The reduction reaction behaviors of the lithium-doped (Co, Mg)O solid solution are shown in Fig. 6. The behavior of the undoped (Co, Mg)O solid solution is also shown in Fig. 6. From Fig. 6, as the doping concentration of the lithium ion increased, the temperature from which reduction started drastically decreased, except that of Sample No. 4. The reduction behavior also drastically changed, except that of Sample No. 4; the weight loss progressed rapidly at the temperature from which reduction started. Figure 7 shows the weight change behavior as a function of time. In the case of Sample No. 4, the reduction

behavior obeyed a parabolic law, and in the case of Sample No. 5 and No. 6, the behavior obeyed a linear law as follows:

$$\Delta m = k_1 t \quad (11)$$

where  $k_1$  is the linear reduction reaction rate constant. The reduction reaction rate constant at each temperature was examined to obtain Arrhenius plots, as shown in Fig. 8 (Table II summarizes the activation energy and frequency factor from the Arrhenius plots). The linear law of the reduction reaction is

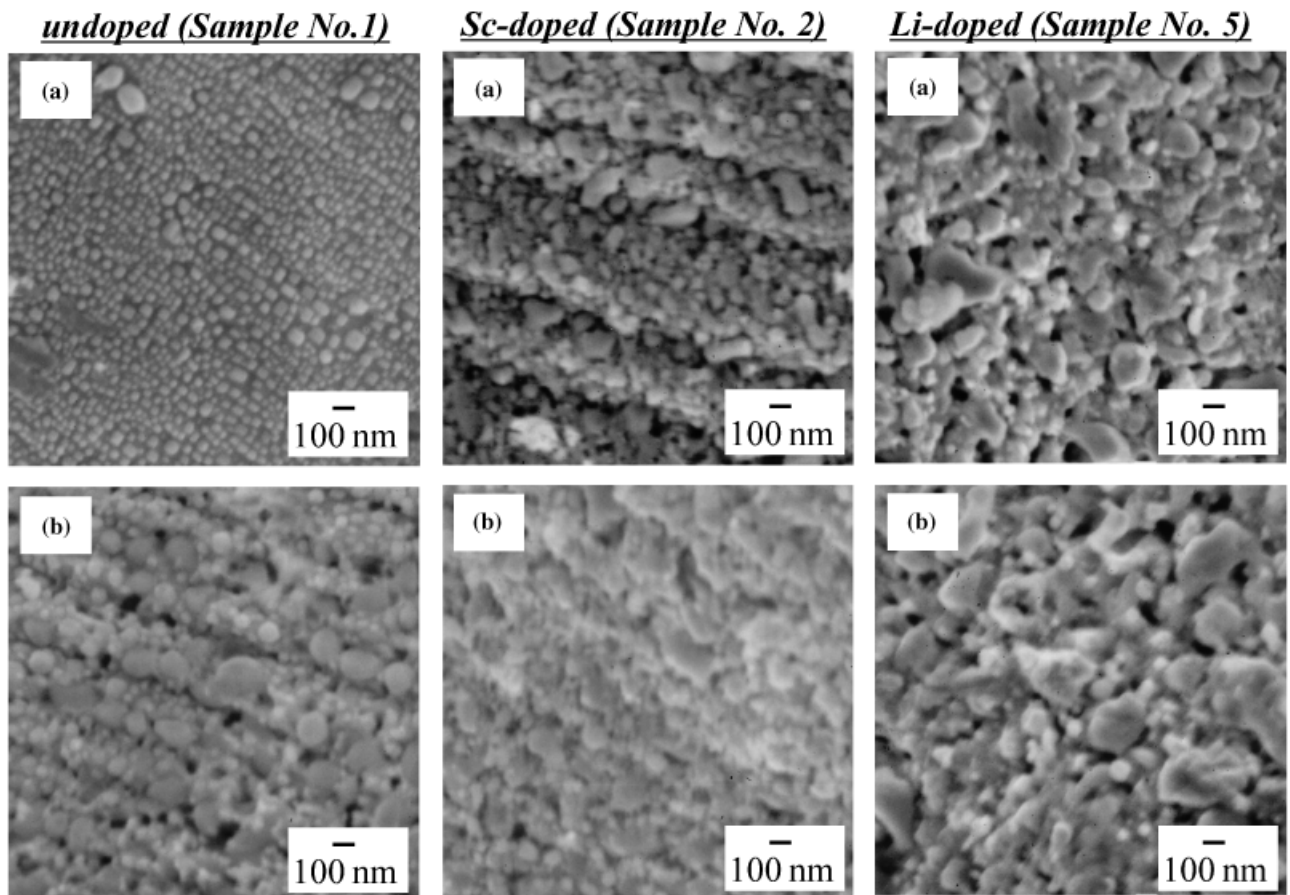


**Fig. 10.** Scanning electron microscopy micrographs of the scandium-doped, lithium-doped, and undoped (Co, Mg)O samples after the hydrogen reduction; (a) after 2.5–3 wt% reduction, (b) after 5.5–6 wt% reduction at 1000°C for the undoped sample, and at 750°C for the doped samples.

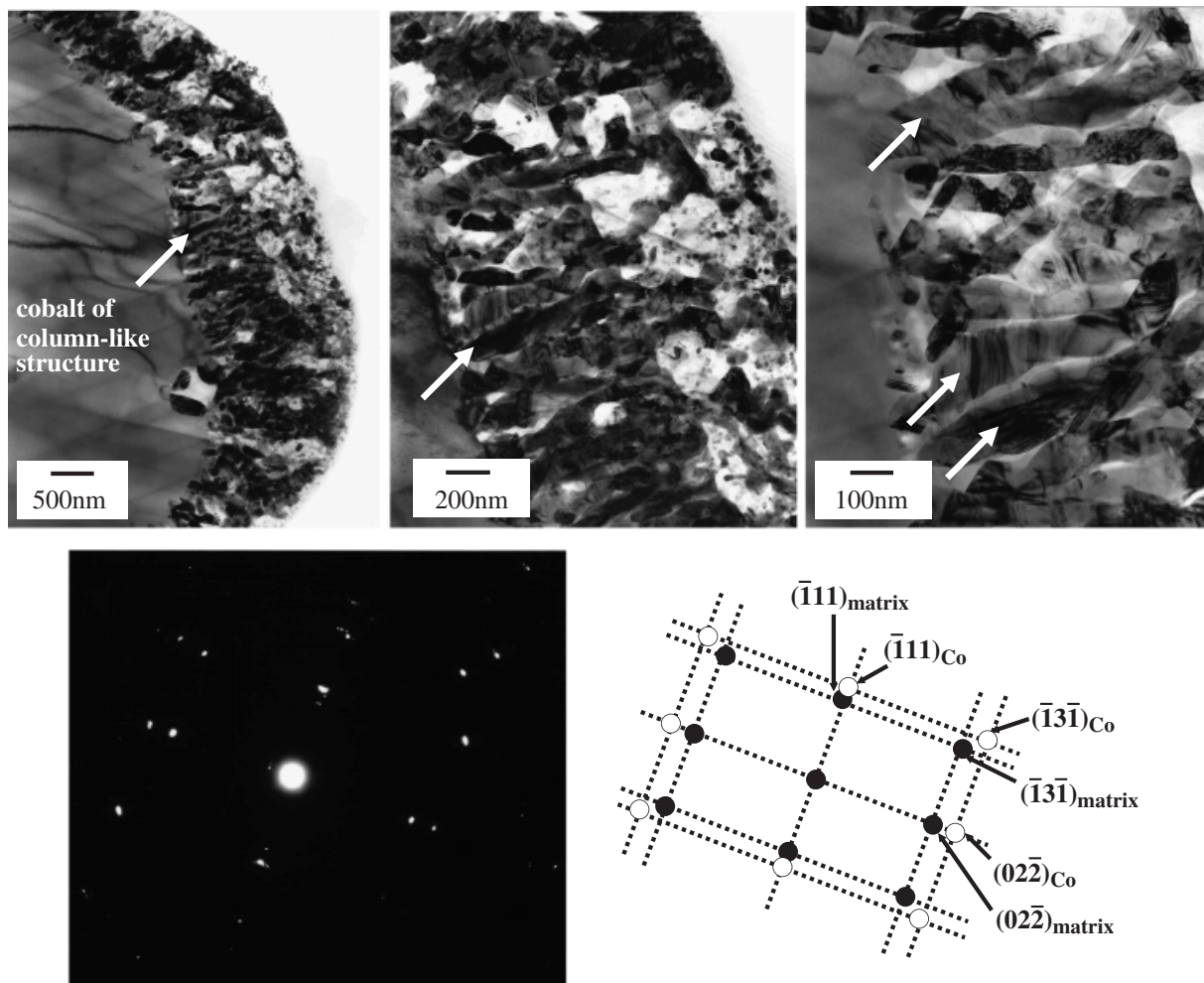


**Fig. 11.** Transmission electron microscopy micrographs of the scandium doped (Co, Mg)O (Sample No. 2) after the hydrogen reduction at 750°C (after 5.5–6 wt% reduction). White arrows indicate the deposited cobalt of a nano column-like structure. Diffraction pattern in the  $[2\bar{1}\bar{1}]$  zone axis is also shown in the  $\varnothing 400$  nm areas including the deposited cobalt particles and matrix.

thought to be realized when interface reaction controls the reaction, while parabolic law is thought to be realized when diffusion controls the reaction. In the case of the quite small doping concentration of lithium ion, the reduction behavior obeyed a parabolic law, and diffusion was rate controlling. On the other hand, in the case of the large doping concentration of lithium ion, the reduction behavior obeyed a linear law, and the interface reaction was rate controlling. In this case of the linear law, the reduction reaction progressed more rapidly than in the case of the parabolic law. This rapid reduction in the linear law could have been caused by the following reason: as the doping concentration of lithium ion increased, oxygen ion vacancy increased and oxygen ion may have diffused faster. The diffusion of cobalt ion of (Co, Mg)O would also be relatively fast, because the concentration of cobalt ion into (Co, Mg)O was high (the ratio of cobalt to magnesium was about 4) [Correction added after online publication 10 August 2007; “metal cation” and “since it could diffuse through the oxygen ion vacancy because of its small ion radius compared with that of oxygen ion.” deleted]. Therefore the diffusions of both metal cation (cobalt ion) and oxygen ion would be relatively fast, and the interface reaction but not diffusion would be rate controlling in the reduction reaction, which caused the rapid reduction reaction.

### (3) Morphology After Reduction

Figure 9 shows the XRD patterns of the doped and undoped (Co, Mg)O samples before and after the reduction (Fig. 9(a) is

before the reduction. Figures 9(b) and (c) are after 2.5–3 and 5.5–6 wt% reductions, respectively). In all cases, a metallic cobalt phase as well as (Co, Mg)O solid solution phase after the reduction was observed, and the cobalt phase increased as the amount of reduction increased.

Figure 10 shows SEM micrographs of the doped and undoped (Co, Mg)O samples after the hydrogen reduction. Figure 10(a) shows SEM micrographs after 2.5–3 wt% reduction and Fig. 10(b) shows them after a 5.5–6 wt% reduction. In the case of the undoped sample, cobalt nanoparticles 20–100 nm in diameter were dispersed on the surface of the ceramic after 2.5–3 wt% reduction, and more particles of larger sizes were dispersed and the surface morphology was rough after 5.5–6 wt% reduction. The rough surface was thought to be caused by the drastic reduction at the surface of the ceramic. This drastic reduction was also observed in both cases of (Co, Mg)O with a scandium dopant and a lithium dopant even after 2.5–3 wt% reduction. This is supported by the drastic reduction behavior (Figs. 3 and 6). Figures 11 and 12 show TEM micrographs of the scandium doped and lithium doped (Co, Mg)O after the hydrogen reduction (after 5.5–6 wt% reduction), respectively. In the case of the scandium doping, the reduced cobalt was grown from the surface toward the inside of the ceramic, and cobalt of a nanocolumn-like structure was formed (Fig. 11). The diameter of the column was about 100 nm. The scandium ion of the doping oxide increased the metal cation diffusion rate toward the surface of the ceramic and columnar growth likely occurred from the surface. On the other hand, in the case of the lithium doping, the reduced cobalt particles were dispersed from the

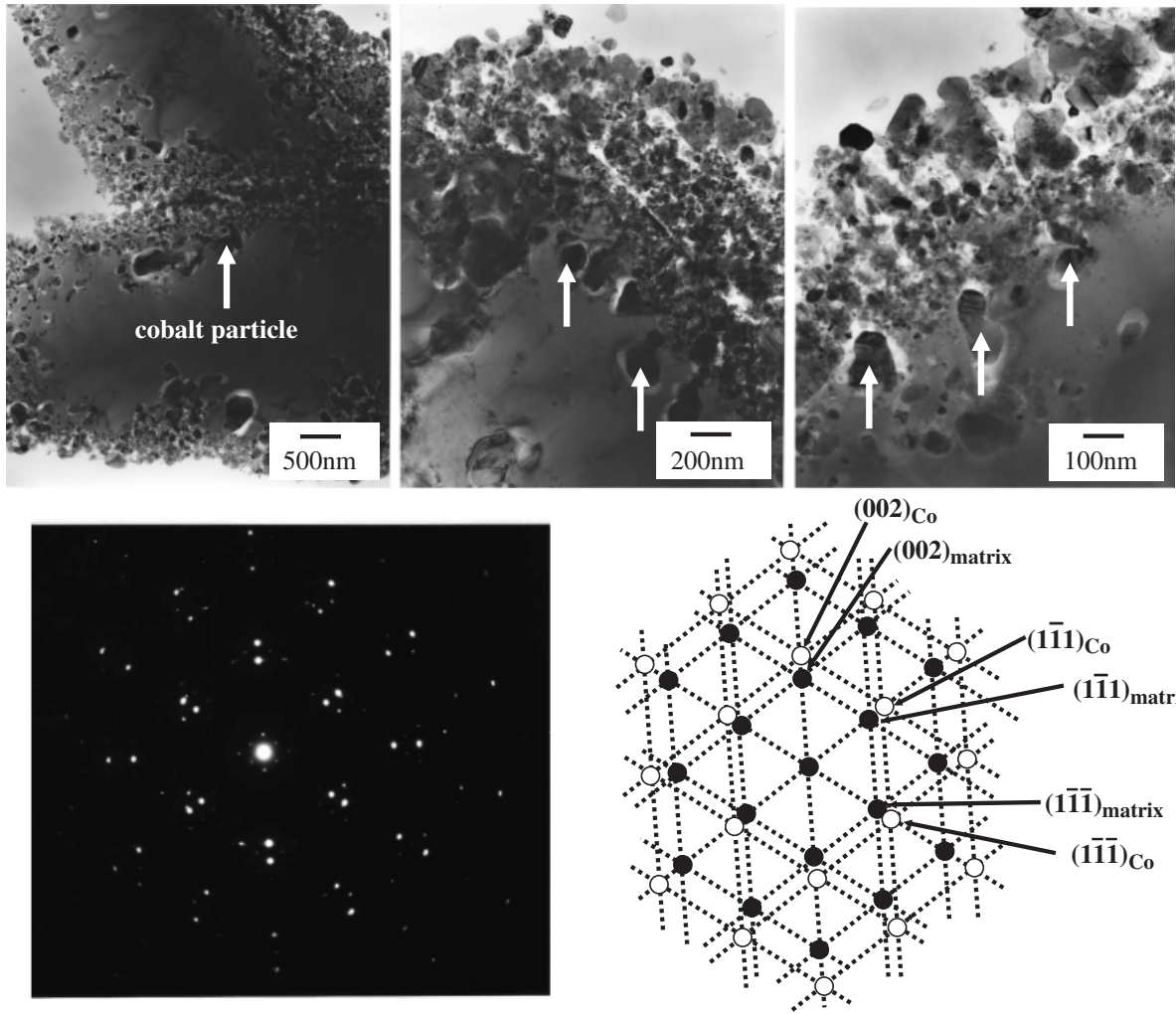


**Fig. 12.** Transmission electron microscopy micrographs of the lithium doped (Co, Mg)O (Sample No.5) after the hydrogen reduction at 750°C (after 5.5–6 wt% reduction). White arrows indicate the deposited cobalt particles. The diffraction pattern in the  $[110]$  zone axis is also shown in the  $\varnothing 400$  nm areas including the deposited cobalt particles and matrix.

surface toward the inside without excessive growth although cobalt had a relatively large size difference (Fig. 12). The diameters of the deposited cobalt particles were 10–200 nm. The lithium ion of doping oxide increased the oxygen ion vacancy, and the interface reaction (not diffusion) was rate controlling in the hydrogen-reduction reaction. Therefore, rapid reduction from the surface toward the inside occurred and many cobalt particles were dispersed toward the inside.

Although the structures realized in the present research were not so refined, there is a possibility to control the variation of the structures of metal/ceramic nanocomposites in the selective reduction reaction of the solid solution. This variation of the structures could control the electric and magnetic properties such as magneto-resistance and magnetization behavior; for example, a nano-granular structure of ferromagnetic particles and antiferromagnetic matrix could enhance the magneto-resistance effect, or the columnar structure could enhance the magnetic anisotropy by its large shape anisotropy.

From TEM diffraction patterns of Figs. 11 and 12, almost all of the deposited cobalt particles in one matrix grain were oriented in the same direction as that of the matrix like  $(100)_{\text{Co}}// (100)_{\text{matrix}}$  and  $(010)_{\text{Co}}// (010)_{\text{matrix}}$ . The lattice constants of MgO, CoO, and cobalt are 4.21, 4.26, and 3.54, respectively. The difference in the lattice constants between the (Co, Mg)O solid solution and the deposited cobalt may induce a strain in the interface between the matrix and the deposited cobalt. This strain could modify the electric and magnetic properties such as

magneto-resistance behavior and magnetization curve, and may be favorable for some applications; for example the magnetic anisotropy can be increased by the inverse magnetostrictive effect.

#### IV. Conclusions

A novel metal/ceramic nanocomposite was synthesized by defect control in a selective reduction reaction of a complex solid solution. The defect type of a (Co, Mg)O solid solution was controlled by doping oxides with different valencies. Doping of scandium in (Co, Mg)O increased the metal cation vacancy, and doping of lithium changed the dominant defect from a metal cation vacancy to an oxygen ion vacancy. These changes in the dominant defects strongly affected the hydrogen-reduction reaction behaviors as well as material morphologies after the reaction. In the case of scandium doping, the diffusion was rate controlling in the reduction reaction, and metals of a nanocolumn-like structure were highly dispersed into the matrix. On the other hand, in the case of lithium doping, the interface reaction was rate controlling in the reaction, and metal nanoparticles were highly dispersed into the matrix.

It was found that material morphologies in the metal/ceramic nanocomposite could be varied by controlling the defect of the solid solution. A more refined morphology could be obtained by controlling the composition of the solid solution, grain size of the solid solution oxide, and reduction condition.

## References

- <sup>1</sup>J. Narayan and Y. Chen, "Physical Properties of Oxides Containing Metal Precipitates Part II," *Philos. Mag. A*, **49** [4] 475–92 (1984).
- <sup>2</sup>J. A. Smith, P. Limthongkul, L. Hartsuyker, S. Y. Kim, and S. L. Sass, "Magneto-Optical Properties of Ni–MgO and Co–MgO Nanocomposite Films Obtained by Partial Reduction Reactions," *Mat. Res. Soc. Symp. Proc.*, **475**, 245–50 (1997).
- <sup>3</sup>J. A. Smith, P. Limthongkul, L. Hartsuyker, S. Y. Kim, and S. L. Sass, "Magneto-Optical Properties of Nanocomposite Films Obtained by Partial Reduction of (Ni, Mg)O and (Co, Mg)O Solid Solutions," *J. Appl. Phys.*, **83** [5] 2719–26 (1998).
- <sup>4</sup>T. Suetsuna, S. Suenaga, and T. Fukasawa, "Monolithic Cu–Ni-Based Catalyst for Reforming Hydrocarbon Fuel Sources," *Appl. Catal. A*, **276**, 275–9 (2004).
- <sup>5</sup>T. Fukasawa, T. Suetsuna, K. Harada, and S. Suenaga, "Catalytic Performance of Metal Nanoparticles Supported by Ceramic Composite Produced by Partial Reduction of Solid Solution with Dopant," *J. Am. Ceram. Soc.*, **88** [10] 2938–41 (2005).
- <sup>6</sup>K. Harada, T. Fukasawa, T. Suetsuna, and S. Suenaga, "Small Reformer for Steam Reforming of Methanol Using Ni Nanoparticles on a Ceramic Surface," *Trans. Mater. Res. Soc. Jpn.*, **30** [4] 987–9 (2005).
- <sup>7</sup>T. Suetsuna, S. Suenaga, T. Fukasawa, and K. Harada, "Development of Metal/Ceramic Nanocomposite," *Bull. Jpn. Electron. Mater. Soc.*, **37**, 40–3 (2006) (in Japanese).
- <sup>8</sup>J. Narayan, Y. Chen, R. M. Moon, and R. W. Carpenter, "Characterization of Metal Precipitates in Magnesium Oxide Part I," *Philos. Mag. A*, **49** [2] 287–300 (1984).
- <sup>9</sup>D. L. Ricoult and H. Schmalzried, "Internal Reactions in the (Mg, Me)O System," *J. Mater. Sci.*, **22**, 2257–66 (1987).
- <sup>10</sup>M. Backhaus-Ricoult and D. Ricoult, "Electron Microscopy of Internally Reduced (Mg, Ni)O," *J. Mater. Sci.*, **23**, 1309–16 (1988).
- <sup>11</sup>J. A. Smith, P. Limthongkul, and S. L. Sass, "Microstructures and Mechanical Properties of Ni–MgO Composites Formed by Displacement and Partial Reduction Reactions," *Acta Mater.*, **45** [10] 4241–50 (1997).
- <sup>12</sup>S. Suenaga, T. Suetsuna, K. Harada, and T. Fukasawa, "In Situ Formation of Metal Nanoparticles on Ceramic Surface," *J. Am. Ceram. Soc.*, **87** [5] 963–6 (2004).
- <sup>13</sup>F. Henriksen and W. D. Kingery, "The Solid Solubility of  $\text{Sc}_2\text{O}_3$ ,  $\text{Al}_2\text{O}_3$ ,  $\text{Cr}_2\text{O}_3$ ,  $\text{SiO}_2$ , and  $\text{ZrO}_2$  in MgO," *Ceramurgia Int.*, **5** [1] 11–7 (1979). □